# Quasi-static Loads Analysis of a 5-bladed Rotor in Maneuver using CFD/CSD Coupling

Seonghyun Hong, aerohong721@gmail.com, Konkuk University (Republic of Korea)

Sung Jung, snjung@konkuk.ac.kr, Konkuk University (Repubilc of Korea)

Kiro Kim, kork2r@naver.com, Konkuk University (Repubilc of Korea)

Soo Hyung Park, pish@konkuk.ac.kr, Konkuk University (Republic of Korea)

Da-woon Lee, downl3824@snu.ac.kr, Seoul National University (Repubilc of Korea)

Joonbae Lee, joonbae.lee@koreaaero.com, Korea Aerospace Industries (Republic of Korea)

## Abstract

The airloads and structural loads of Light Civil Helicopter (LCH) rotor in a pull-up maneuver are investigated using a coupled approach between the computational structural dynamics (CSD) and computational fluid dynamics (CFD) methods. The LCH rotor characterized by 5-bladed system with elastomeric bearing and inter-bladed damper is modeled in the structural dynamics analysis. The periodic rotor solution along with its converged CFD/CSD delta airloads for steady level flight ($\mu$ = 0.287) is used to perform the transient maneuver analysis. The resulting vehicle attitude angles and velocity profiles are then prescribed for the quasi-static maneuver analysis of the rotor. The predicted section airloads, vortex trajectories, angle of attack (AOA)distributions, and structural moments at specified instants and spatial locations are compared between transient CSD-alone predictions and quasi-static CFD/CSD maneuver results. It is demonstrated that CFD/CSD coupled results indicate more pronounced dynamic stall peaks and stronger 5 /rev oscillations on structural moments than those by the CSD-alone approach.

## 1. INTRODUCTION

Recently, KAI (Korea Aerospace Research Industries, LTD) is developing a 5 ton-class helicopter named LCH (Light Civil Helicopter) which is based on the earlier platform of H155B by AH (Airbus Helicopter) [1]. Figure 1 shows the conceptual drawing of LCH. The rotor is 5-bladed articulated rotor with the radius and chord of 6.3 m and 0.385 m, respectively, and equipped with an interbladed damper along with an elastomeric bearing to accommodate the desired pitch control input.



In the stage of new helicopter design, detailed loads analysis particularly at or near the extreme corner points in the flight envelope is necessary to ensure the safe operation of an aircraft. It is conceived that helicopter structures experience some of the most severe loadings and vibrations during maneuver flights [2].

Accurate and reliable predictions of airloads and structural loads especially in maneuvering flight is challenging because of highly nonlinear and transient nature involved in the analysis. Among others, three-dimensional transonic effects in the advancing side, reversed flow and dynamic stall in the retreating side, and blade-vortex interaction events in the vicinity of the rotor disk are the crucial parts of the aeromechanics analysis that should be countered correctly. Highly unsteady air flows and large blade elastic deformations make the analysis more complicated and often require the most-sophisticated solution technologies such as CFD/CSD coupling to tap correctly the



Presented at 45th European Rotorcraft Forum, Warsaw, Poland, September 17-20, 2019

complex phenomena and gain detailed physics associated with the aeroelastic behavior of the vehicle in motion.

In the rotorcraft aeromechanics analysis, CFD/CSD coupling is rooted in Tung et al. [3] where two separate codes (i.e. CFD and CSD solvers) are loosely coupled (LC) by transferring data per periodic base. This pioneering approach later invokes researchers to revisit and tackle the unsolved rotorcraft aeroelastic problems particularly in relation to UH-60A airloads program mentioned in Bousman [4], resulting in significant advances in the prediction capability and enhancing the degree of understanding for many engineering problems met in the rotorcraft aeromechanics fields [5-9]. The alternative method is a tight coupling (TC) approach where the blade motion (CSD) and airloads (CFD) data are exchanged at every time step, hence the periodicity assumption in LC algorithm is abandoned for general, time accurate analysis solutions. Bhagwat et al. [2] applied TC approach to examine aerodynamic and structural loads of UH-60A rotor in the UTTAS pull-up maneuver flight. The simulation results demonstrate significantly improved correlations with the flight test data as opposed to the CSD-alone based approach, but with the consumption of heavy computational resources. Interestingly, they compared the accuracy of air and structural loads of the rotor (during the peak maneuver events) between LC and TC approaches. It is reported that no significant deviations between the two different methodologies are found. In either approach, the measured flight data on the rotor pitch controls and the hub motions are used and prescribed for the pull-up maneuver analysis. It should be mentioned that TC scheme is more straightforward and rigorous than its LC counterpart. However, the time lagging between CFD and CSD codes cannot be avoided. Furthermore, it is difficult to manage the trim. Battey and Sankar [10] applied LC algorithm successfully for the evaluation of maneuver loads of UH-60A rotor.

In the present work, the LC approach is employed to evaluate the airloads and structural loads of the 5-bladed LCH rotor in a pull-up maneuver. To this purpose, either CAMRAD II [11] or KFLOW [12] code is used for the analysis. It is noted that the same LC approach has been successfully demonstrated to validate HART II test data [7-8,13] and those of its predecessor program HART [9]. A 3.2g UTTAS pull-up maneuver condition is selected for the study. Since the measured data on vehicle attitude angles and flight trajectories of the maneuver profile are not available for the LCH rotor, the flight dynamics simulation results predicted using CAMRAD II with converged CFD/CSD delta airloads are used instead to carry out the maneuver loads analysis. The proposed algorithm is applied to predict airloads, vortex trajectories, and structural loads of the rotor and in-depth discussions are made to evaluate the aeromechanics characteristics at maneuvering flight regime.

## 2. LCH ROTOR MODEL

### 2.1. CSD Model

A rotorcraft computational dynamics code CAMRAD II [11] is used to analyze the LCH rotor. The code is built based on multibody dynamics, nonlinear finite elements, and different level of aerodynamic models. For the structural model, the blades are discretized into a series of beam finite elements. The aerodynamic loads acting on the blades are computed using ONERA-EDLIN unsteady airfoil theory combined with C81 airfoil table look-up. A rolled-up free wake model is used for the vortex wake representation while a semi-empirical Beddoes-Leishman model is used for the dynamic stall prediction. Figure 2 shows both the aerodynamic and structural models adopted in the present CSD analysis. The airfoil blade region is divided into 15 non-uniform aerodynamic panels with finer segments being placed toward the blade tip. For the blade structure, a total of 18 beam finite elements are distributed over the blade span. Each beam element consists of 15 degrees of freedom (DOF) with 6 rigid and 9 elastic motions (3 axial, 2 flap, 2 lag, and 2 torsion). The hub model includes pitch horns and their linkage mechanisms along with the lead-lag damper interconnected between the adjacent blades (see Figure 2b). Table 1 summarizes the general properties of LCH rotor. It is remarked that the LCH rotor has articulated hinges co-located at 0.039*R* (blade radius). In CAMRAD II analysis, a pitch link model is employed to accommodate the pitch

control input. The pitch link spring stiffness is not measured and thus determined to match the first torsion frequency which is about 6.0 /rev.

### 2.2. CFD Model

A 3D compressible Euler (or RANS (Reynolds-Averaged Navier-Stokes)) flow solver KFLOW [12] is used for the CFD analysis. For time-accurate flow simulations, the second-order dual-time stepping scheme combined with a diagonalized alternating-directional implicit method is applied to simulations of the unsteady rotor flow fields. The Roe's upwind flux-difference splitting scheme is used to calculate the inviscid flux. The third-order MUSCL interpolation is employed to obtain second-order accuracy.

A moving overlapped Chimera grid system is constructed for the rotating blades and the Cartesian off-body background field. C-H mesh topology grids are formed near the blade surface. Figure 3 shows the computational grid systems used for an isolated, 5-bladed LCH rotor. The blade grids extend 1.5 times of a chord length (*c*) in the normal direction, measured from the blade surface. Fine inner off-body region around the blade grids extends 4*c* upward, 3*c* below from the blade, and 1.5*c* away from the blade tip. The far field boundary is stretched up to 5*R*, centered at the rotor hub. Numerical experiments have shown that the cell spacing of 0.15*c* is appropriate for the off-body background grids. The blade grid has dimensions of 66×99×69 corresponding to the normal, spanwise, and chord wise directions which sums up to 0.43M cells for each blade. The CFD computational grids amounts to a total of 37.2M cells including the near-body blade grids and the off-body background grids for an isolated LCH rotor model.

## 3. MANEUVER ANALYSIS

### 3.1. Pull-up maneuver

The LCH pull-up maneuver scenario is presented in Figure 4. The longitudinal cyclic stick is pulled forward by up to 4.8 degrees to change pitch control angles. The longitudinal stick input begins to rise at 0.2 seconds, reaches the peak value at 0.4 seconds, and stays for the duration of 1.6 seconds, then it decreases to -4.8 degrees to turn back and change further down in the attitudes of the vehicle. The resulting changes in section pitch angles at 0.83*R* due to the pilot stick input are illustrated in Figure 4b. The time period of two seconds corresponds to approximately 11.4 rotor revolutions. The pitch angles become increased by about 2 degrees based from those of the level flight and dropped substantially thereafter. This pull-up input schedule appears to be drastic and results in deep changes in blade loadings and rotor thrust outputs. Figure 5 presents the variation of the effective weight coefficients ($n_z C_w/\sigma$) for the LCH pull-up varied as a function of the advance ratios. Though the aircraft class is quite different from each other, the corresponding ones with UH-60A pull-up maneuver [14] are compared for reference purpose. The McHugh lift boundary is also included to identify the level of thrust generated during the pull-up maneuver flight [15]. Since UH-60 airloads program data are not released to the public, the graph is extracted from Bhagwat et al. [2]. It should be mentioned that both rotors indicate crossing the McHugh boundary leading to severe dynamic stall regions, particularly for LCH rotor. The effective weight coefficient reaches up to maximum 3.18g for LCH case while UH-60A being bounded by 2.1g.

### 3.2. Maneuver analysis methodology

To predict the air and structural loads of a rotor in pull-up maneuver, a time accurate TC scheme is truly desired since the problem is naturally unsteady. However, in this study, it is assumed that each revolution can be approximated as the steady state, leading to a quasi-static condition. This observation has been verified earlier by Bhagwat et al. [2] for the study of UH-60A maneuver loads analysis. The overall flow diagram for the quasi-static LCH maneuver analysis is presented in Figure 6. It is composed of three stages: (1) LC in level flight condition; (2) CSD transient analysis for prescribed vehicle motions; (3) quasi-static maneuver analysis at specific instant of time (revolution) for aeromechanics loads of the rotor. The second stage of the analysis is needed since no measured data on flight dynamics test for LCH have been available so far.

The analysis begins with LC between CFD

and CSD codes in steady level flight condition. The flight speed $\mu$ equals 0.287 as is denoted in Figure 5. The LC run requires about 6 to 8 iteration cycles of transferring data between airloads (CFD) and blade motions (CSD) for the convergence. Figure 7 shows the iteration histories on target forces and moments as well as the resulting trim control angles. A zero moment trim strategy is employed to trim the rotor. Once the convergence is reached, the converged delta airloads are saved for later use in the transient flight analysis. A separate CSD transient analysis with converged trim angles and delta airloads is conducted to find the time histories of LCH motion in maneuver which include vehicle attitude angles and velocity components according to the maneuver scenario. In the transient analysis, the converged delta airloads obtained from LC coupling in level flight are added in the CSD analysis to improve the solution accuracy of its flight dynamics predictions.

Figure 8 shows the time histories of vehicle attitude angles (Figure 8a) and velocity components (Figure 8b) of LCH rotor predicted using the transient CSD analysis with and without the delta airloads obtained from the steady level flight condition. It is observed that the effects of incorporating delta airloads in the transient CSD analysis appear to be substantial as the time (revolution) marches further. From the transient analysis results, the motion angles and blade deformations are averaged for each revolution. The control angles required for each revolution are interpolated from the transient analysis results using the Fourier harmonic series. Figure 8 shows the curve-fitted control angles during the transient pull-up maneuver. It is observed that the waveform is accurately followed when using the Fourier series up to 10th harmonics. Given the prescribed motion data ready during the pull-up maneuver, the CFD time marching analysis or LC approach at specified revolution which is of interest is engaged to perform the maneuver analysis.

## 4. RESULTS AND DISCUSSION

Numerical simulation study for the LCH rotor in the 3.18g pull-up condition is performed using the quasi-static maneuver scheme described in the previous section. Unless otherwise specified, a rolled-up free wake model is used throughout the CSD analysis, whereas in CFD computation, Euler representation of the flow solver is exploited for the efficiency reason.

Figure 10 shows the time history responses on section normal forces $M^2C_n$ and pitching moments $M^2C_m$ computed at 0.875$R$ of LCH blade. Either CSD transient analysis results with delta airloads (red continuous lines) or CFD predictions with prescribed motions (black continuous lines) of the aircraft are presented as a function of rotor revolutions. Since the pull-up input starts at 0.2 seconds (which corresponds to approximately 1.14 rev), CFD results on and after 1 rotor revolution are presented. As can be seen in Figure 10, the two predictions indicate large variations with each other, though the mean values are predicted closely. Specifically, as the revolution increases, the quasi-static CFD analysis catches much stronger peaks with higher harmonic contents which are related to the blade vortex interaction (BVI) events along with dynamic stall peaks apparent in the section pitching moment results, as compared with those of CSD analysis. It is noted that the McHugh's lift boundary is crossed around the 4 to 5 revolutions (see Figure 5), leading to sudden drops in section airloads. Some of the unrealistically large peaks obtained in CFD calculations may be incurred due to the neglect of the viscous fluxes in CFD solver. Taken this fact into account, however, the CFD predictions appear to be captured nicely the fundamental flow characteristic of the rotor encountered during the pull-up maneuver, as is illustrated in the following Figure 11.

Figure 11 shows the Q-criterion plot colored by strengths to visualize the vortex trajectories, viewed from the port side (Figure 11a; positioned at 0.64$R$) and the top (Figure 11b), respectively, during the maneuver flight. The rotor revolutions are varied between the plots. As the maneuver input schedule starts around 1.14 revolutions, the vortex trajectory slowly shifts upwards due to an increased pitch-up motion of the vehicle. Looking at the side trajectory view of 5 to 6 revolutions in Figure 11a shows that most of the vortices formed near the front disk region upshift and travel over the rotor disk and convect downward to interact with the blades positioned rear of the rotor disk. Comparing

this with the top view (Figure 11b) clearly indicates the vortex interaction events with the approaching blades, particularly in the first and the fourth quadrants of the rotor disk. These BVI oscillatory peaks are also clearly predicted in the section normal force and pitching moment results at 87.5% blade radial stations, as depicted in Figure 10. Figure 10 indicates dynamic stall events in the retreating region of the disk. The occurrence of dynamic stall events can be identified by investigating the angles of attack distribution during the rotor revolution.

Figure 12 shows the variation in section angles of attack located either at 0.785*R* or 0.875*R* of the rotor as a function of Mach numbers when the rotor revolutions reaches 7 to 8, respectively. For LCH rotor, three different airfoils based on ONERA's OA-series designs (OA 212, OA 209 and OA 207) are used to construct the blade [1]. The static stall boundaries corresponding to the specific airfoils are denoted in the plot for reference purpose. As can be seen, substantial portions of the blades in the retreating side of the disk are well above the static stall limit which may cause the dynamic stall and explain the existence of strong peaks in the pitching moment signals in Figure 10. It is observed that the outer span position of 0.875*R* indicates deeper dynamic stall than its more inward station at 0.785*R*. This is something not expected considering the distribution of built-in twist angles in the LCH blades where -6.06 degrees of linear twist are used along the blade span. Complex flow pattern met in the respective regions (as observed in Figure 11) affect the local aerodynamic characteristics significantly other than the airfoil geometry factors.

So far, the transient CSD analysis or the quasi-static CFD analysis is performed with the pull-up maneuever scenario. Each method is short in that CSD-alone analysis lacks the critical accuracy that can be exploited to rotor loads and vibration study while CFD analysis is inadequate to deal with the structural loads. Therefore, CFD/CSD LC approach is engaged to predict airloads and structural loads at specified revolution of the rotor. To this end, 4 to 5 revolutions are selected for the evaluation of loads. The convergence history representatively on the delta section normal force $\Delta M^2C_n$ and tip elastic twist are presented in the revolution of 4 to 5. It is determined that the convergence appears to be reached when the 8th iteration cycles are proceeded.

In the following figures, the airloads and structural loads computed using LC analysis are shown against the CSD transient analysis results with rolled-up wake model and delta airloads, respectively. Figure 14 shows the section normal forces $M^2C_n$ and pitching moments $M^2C_m$ obtained at the blade radial station 0.875*R*. Both CSD results predict similar values while CSD transient analysis with delta airloads indicating more oscillations by picking up some of the BVI signals in either the advancing side or the retreating side of the disk. Among others, LC approach appears to predict more harmonics and stronger dynamic stall peaks than its CSD counterpart analyses. LC results show a sudden fall of pitching moment around 300 degrees which has not been predicted in both CSD methods. The loss of lifts predicted with LC analysis in the front region of the rotor disk needs further investigation, however, neither CSD approach predicts this kind of dip in the waveform. Figure 15 shows the comparison of flap bending, lead-lag bending, and torsion moments calculated at 40% blade radial station between CSD and CFD/CSD coupled predictions. A stronger 5 /rev response with higher peak-to-peak values are obtained by LC approach than the two CSD approaches. The lead-lag dampers inter-connected between the blades for LCH rotor are the possible source of the 5 /rev signal. It is interesting to note that the mean values of the LC analysis results are reasonably estimated by CSD-alone approach with rolled-up free wake model. This outcome assures the validity of the present analytical methods proposed for the pull-up maneuver flight. The deviations in the mean for CSD approach with delta airloads are not known and this needs further study for clarification.

## 5. CONCLUSION

In this study, a quasi-static CFD/CSD maneuver analysis was performed to investigate the airloads and structural loads of LCH rotor in a pull-up maneuver. Due to the lack of measured flight data at the present instant, the analysis began with LC approach

in steady level flight condition ($\mu$ = 0.287). The converged delta ailoads from the level flight condition were fed into CAMRAD II for the transient maneuver analysis. The resulting vehicle motions data were then prescribed to enable the overall quasi-static maneuver simulation and to evaluate the detailed flow behaviour of the rotor. Finally, the LC approach is engaged for the rotor at specific revolution to examine the blade motions, airloads, and structural loads.

The predicted airloads from the quasi-static CFD/CSD maneuever analysis were compared with those of CAMRAD II transient analysis with roll-up free wake model. The comparison results showed that much stronger dynamic stall peaks with higher peak-to-peak airloads signals were captured with the LC approach than its CSD counterpart results. The CFD/CSD results on structural loads of LCH rotor indicated much larger contribution of 5 /rev harmonics than CSD-alone predictions, possibly due to the inter-bladed damper. The stronger BVI oscillatory peaks in the CFD transient results were also identified using the Q-criterion plot colored by strengths. The vortices shifted upward due to the pitch-up during the initial pull-up profile and its later encounter with the blades in the rear portion of the disk attributed to the stronger interactions.

So far, the viscous effects have been neglected in the CFD predictions. The future study will include the viscosity of the flow along with the coverage of longer time periods for the maneuver flight.

## Acknowledgements

This work was supported by the National Research Foundation of Korea (NRF) grant funded by the Korea Government (2018R1A4A1024191). This research was supported by Basic Science Research Program through NRF funded by the Ministry of Education, Science and Technology (2017R1D1A1A09000590).

## References

[1] Lee, J. B., Kang, S. N., Lee, S. K., Im, D. K., Kang, H. J., and Lee, D. J., “Development of Improved Rotor Blade Tip Shape using Multidisciplinary Design Analysis and Optimization,” *44th European Rotorcraft Forum*, Delft, The Netherlands, Sept. 19-20, 2018.

[2] Bhagwat, M. J., Ormiston, R. A., Saberi, H. A., and Xin, H., “Application of Computational Fluid Dynamics/Computational Structural Dynamics Coupling for Analysis of Rotorcraft Airloads and Blade Loads in Maneuvering Flight,” *Journal of the American Helicopter Society*, Vol 57, No. 3, 2012, pp. 1-21.

[3] Tung, C, Caradonna, F. X., and Johnson, W., “The Prediction of Transonic Flows on an Advancing Rotor,” *Journal of the American Helicopter Society*, Vol. 31, No. 3, July 1986, pp. 4-9.

[4] Bousman, W. G., “Putting the Aero Back into Aeroelasticity,” *Eighty ARO Workshop on Aeroelasticity of Rotorcraft Systems*, University Park, PA, Oct. 18-20, 1999.

[5] Potsdam, M., Yeo, H., and Johnson, W., “Rotor Airloads Prediction using Loose Aerodynamic/ Structural Coupling,” *Journal of Aircraft*, Vol. 43, No. 3, 2006, pp. 732-742.

[6] Yeo, H., Potsdom, M., Ortun, B., and Truong, K. V., “High-Fidelity Structural Loads Analysis of the ONERA 7A Rotor,” *Journal of Aircraft*, Vol. 54, No. 5, 2017, pp. 1825-1839.

[7] Jung, S. N., Sa, J. H., You, Y. H., Park, J. S., and Park, S. H., "Loose Fluid-Structure Coupled Approach for a Rotor in Descent Incorporating Fuselage Effects," *Journal of Aircraft*, Vol. 50, No. 4, July 2013, pp. 1016-1026.

[8] Jung, S. N., You, Y. H., Kim, J W., Sa, J. H., Park, J. S., and Park, S. H., "Correlation of Aeroelastic Responses and Structural Loads for a Rotor in Descending Flight," *Journal of Aircraft*, Vol. 49, No. 2, Mar.-Apr. 2012.

[9] You, Y. H., Na, D. H., and Jung, S. N., “Improved Rotor Aeromechanics Predictions Using a Fluid Structure Interaction Approach” *Aerospace Science and Technology*, Vol. 73, 2018, pp. 118-128.

[10] Battey, L. S., and Sankar, L. N., “A Hybrid Navier-Stokes / Viscous Vortex Particle Wake Methodology for Modeling Maneuver Loads,” *44th European Rotorcraft Forum*, Delft, The Netherlands, Sept. 19-20, 2018.

[11] Johnson, W., CAMRAD II: Comprehensive Analytical Model of Rotorcraft Aerodynamics and Dynamics, Johnson Aeronautics, Palo Alto, CA, 1992.

[12] Kim, J. W., Park, S. H., and Yu, Y. H., “Euler and Navier-Stokes Simulations of Helicopter Rotor Blade in Forward Flight Using an Overlapped Grid Solver,” *19th AIAA CFD Conference*, San Antonio, TX, June 2009.

[13] Smith, M. J., Lim, J. W., van der Wall, B. G., Baeder, J. D., Biedron, R. T., Boyd Jr., D. D., Jayaraman, B., Jung, S. N., and Min, B.-Y.,

"The HART II International Workshop: An Assessment of the State of the Art in CFD/CSD Prediction," *CEAS Aeronautical Journal*, Vol. 4, No. 4, 2013, pp. 345–372.

[14] Yeo, H., "Investigation of Rotor Airloads and Structural Loads in Maneuvering Flight," *American Helicopter Society 64th Annual Forum*, Montreal, Canada, Apr. 29 – May 1, 2008.

[15] McHugh, F. J., Clark, R., and Solomon, M., "Wind Tunnel Investigation of Rotor Lift and Propulsive Force at High Speed – Data Analysis," *NASA CR 145217-1*, Oct. 1977.

| Properties | Values |
|---|---|
| Number of blades | 5 |
| Radius | 6.3m |
| Mean chord length | 0.385m |
| solidity | 0.0972 |
| Lock number | 7.4319 |
| Rotational speed | 350 rpm |

Table 1 General properties of LCH rotorcraft

*Figure 1 Conceptual view of LCH [1]*

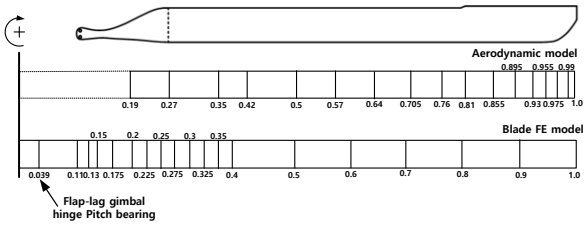


(a) CSD model of LCH rotor

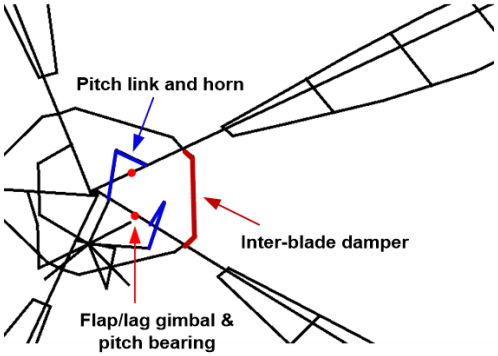


(b) Hub structural model of LCH rotor

*Figure 2 Blade and hub model of LCH rotor*

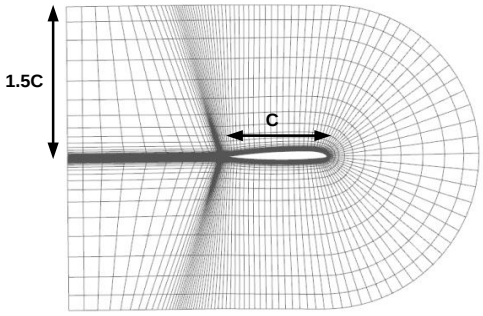


(a) Blade grid system

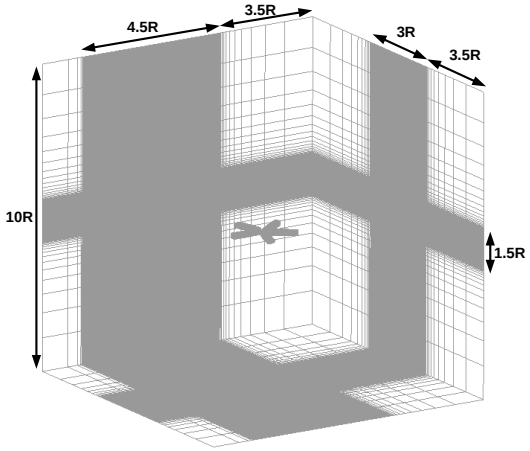


(b) Overall grid system for isolated rotor

*Figure 3 Computational grid system for LCH rotor*

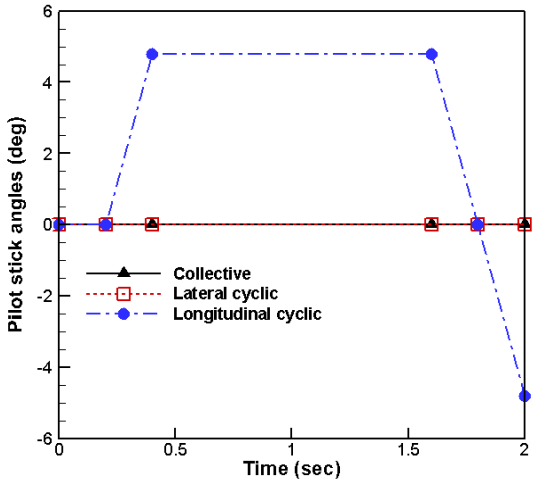


(a) Pilot stick input schedule

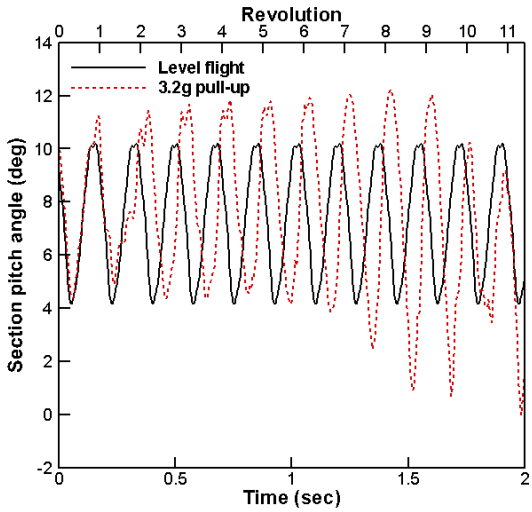


(b) Section pitch angle at 0.83*R*

*Figure 4 LCH pull-up maneuver scenario*

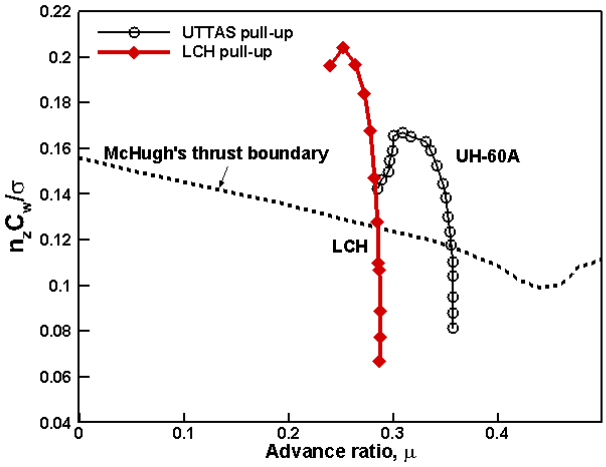


*Figure 5 Change of blade loadings during pull-up maneuver*

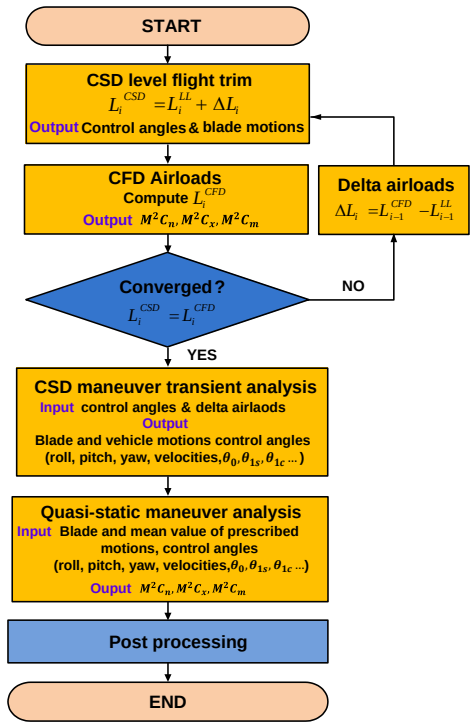


*Figure 6 CFD/CSD coupling algorithm for maneuver analysis*

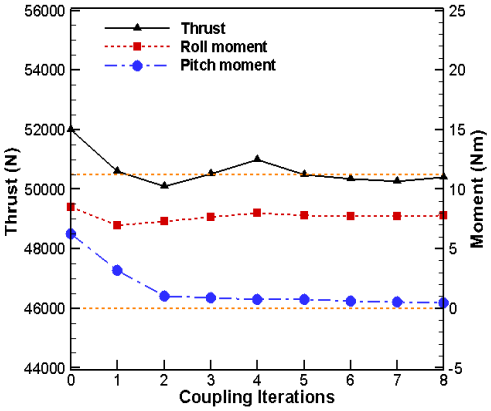


(a) Target forces and moments (CFD)

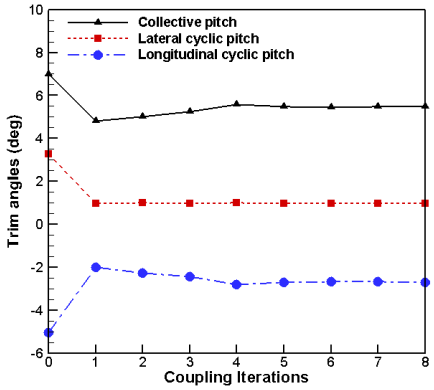


(b) Control trim angles (CSD)

*Figure 7 CFD/CSD convergence history of LCH rotor in cruise flight ($\mu$ = 0.2872)*

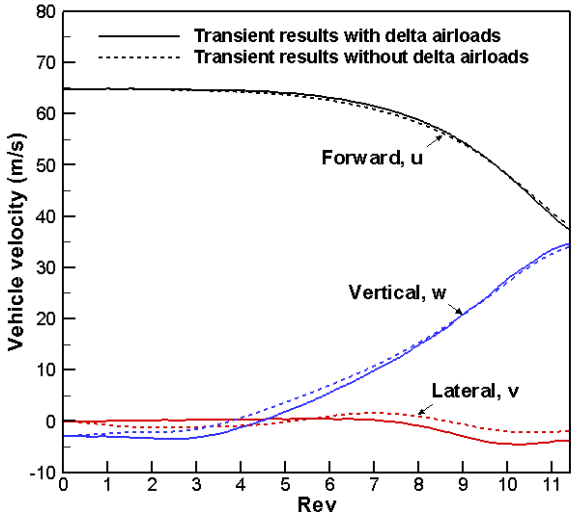


(a) Vehicle attitude angles

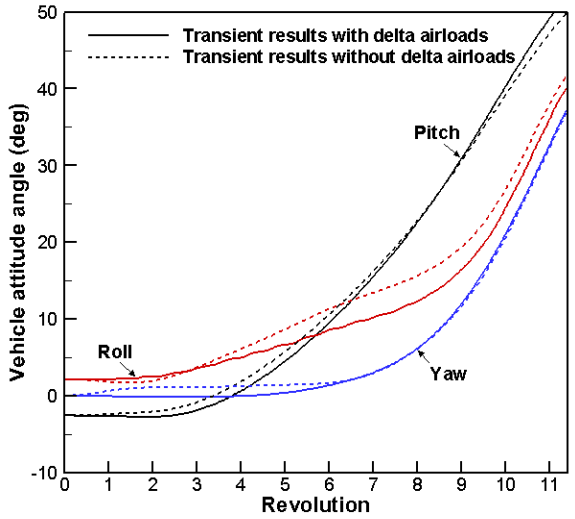


(b) Vehicle velocity

*Figure 8 Vehicle attitude angles and velocity profiles computed using CAMRAD II*

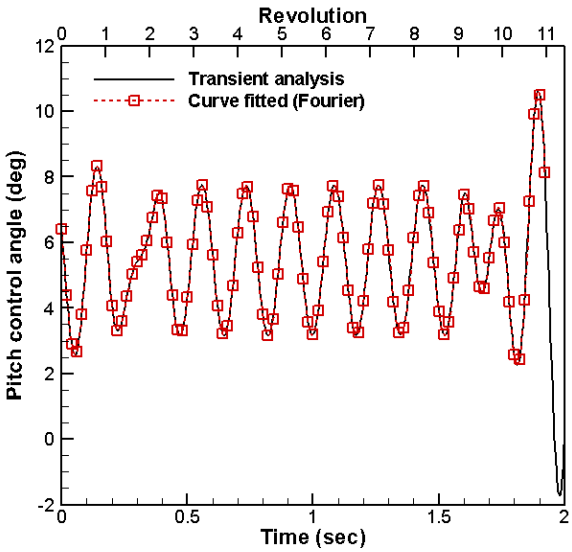


*Figure 9 Pitch control angles converted to Fourier series*

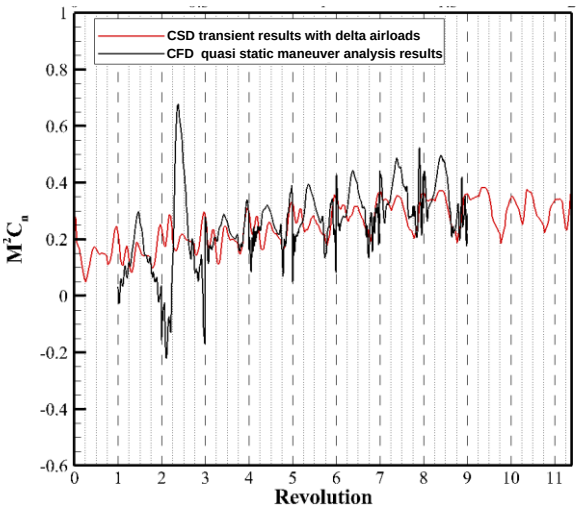


(a) Normal force at 0.875*R*

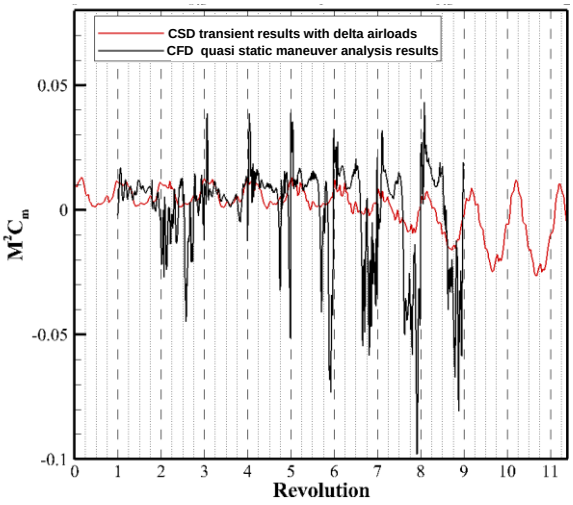


(b) Pitching moment at 0.875*R* (mean removed)

*Figure 10 Comparison of section airloads of LCH rotor during pull-up maneuver*

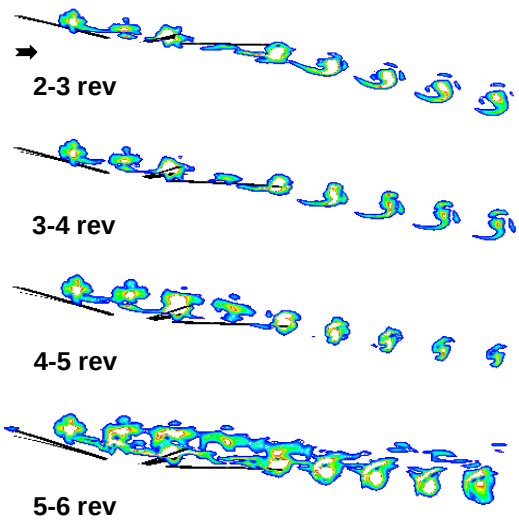


(a) Side view positioned at 0.64*R*

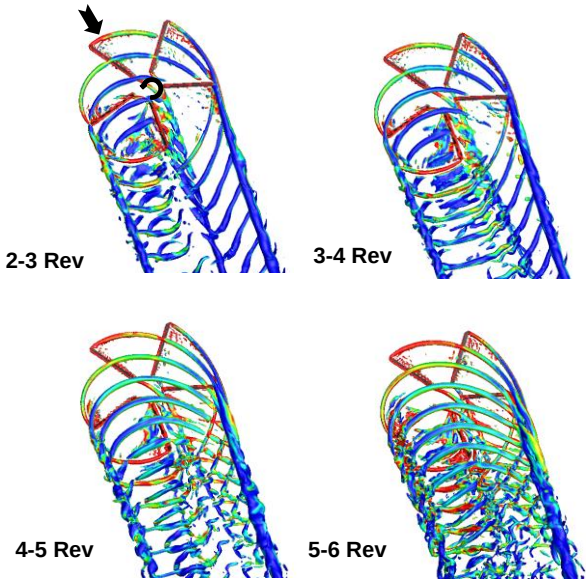


(b) Top view

*Figure 11 Q-criterion plot for vortex trajectory*

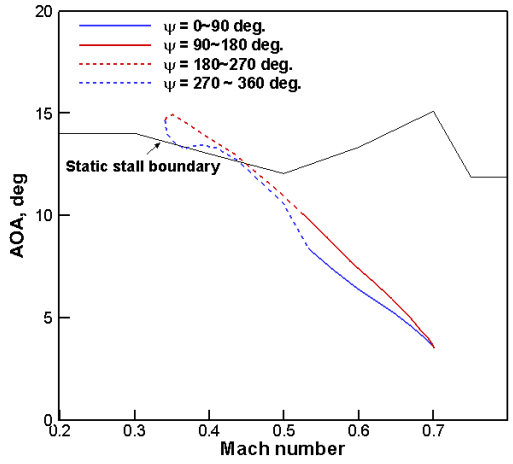


(a) Section angle of attack at 0.785*R* (OA 209)

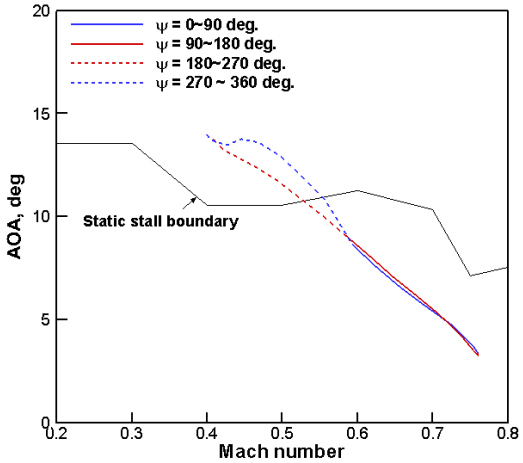


(b) Section angle of attack at 0.875*R* (OA 207)

*Figure 12 Variation of section angles of attack for 7 to 8 revolutions*

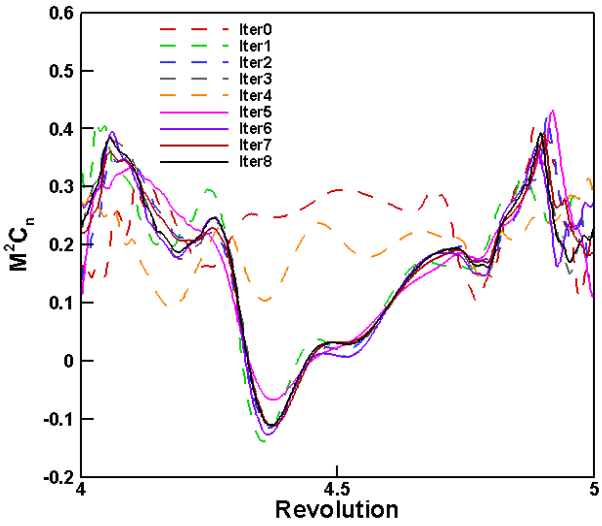


(a) Delta section normal force $\Delta M^2 C_n$ (0.875R)

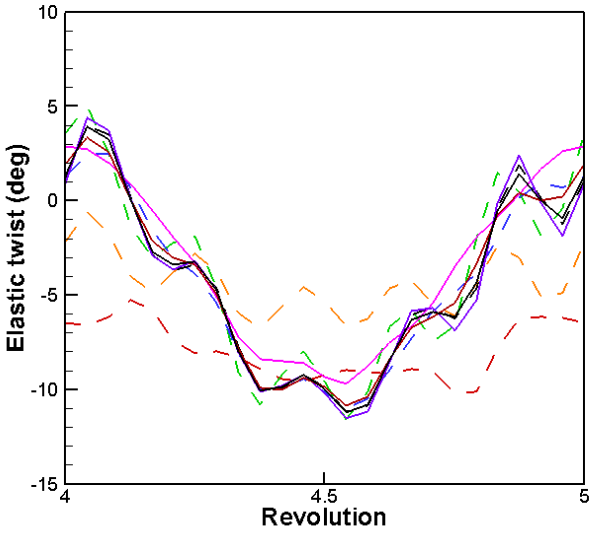


(b) Tip elastic twist

*Figure 13 Convergence history of section airloads and blade motions of LCH rotor in manuver for 4 to 5 revolutions*

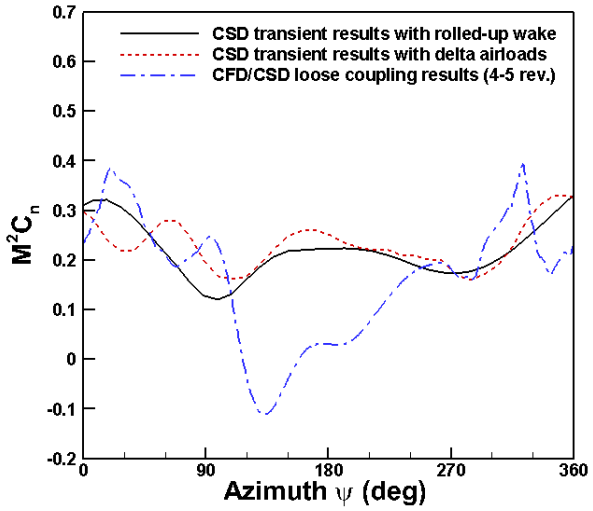


(a) Section normal force

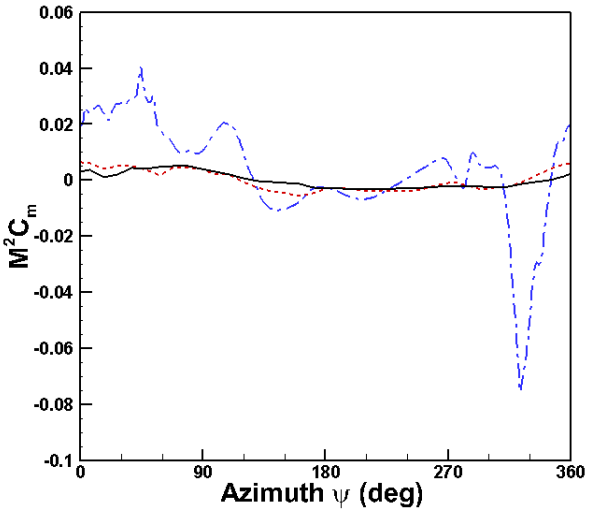


(b) Section pitching moment (mean removed)

*Figure 14 Comparison of section airloads at 0.875R of LCH rotor in maneuver for 4 to 5 revolution*

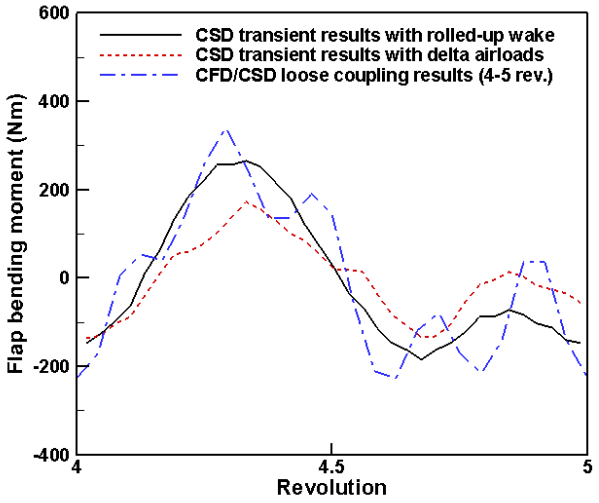


(a) Flap bending moment

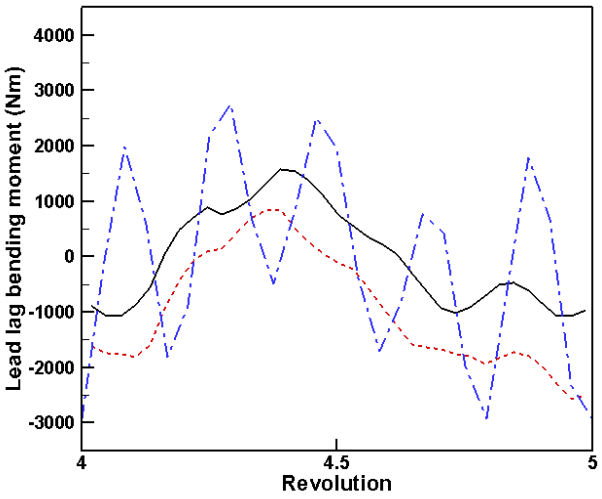


(b) Lead lag bending moment

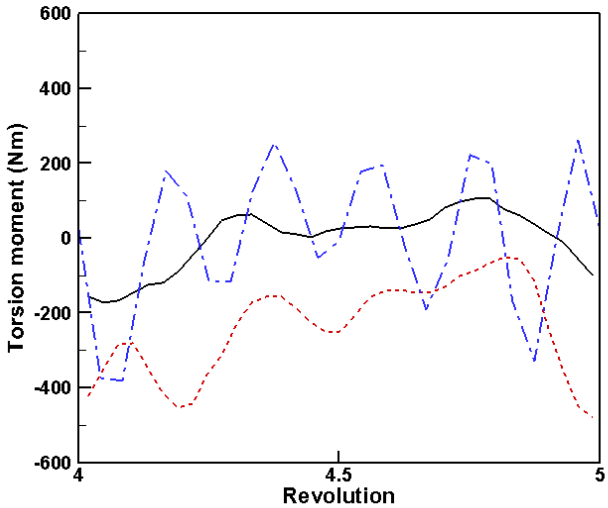


(c) Torsion moment

*Figure 15 Comparison of structural loads at 0.4R of LCH rotor in maneuver for 4 to 5 revolutions (mean removed)*